

A simple sonochemical approach of Mn²⁺ doped ZnO nanopowder: structural, optical and magnetic studies

B. Babu¹ · E. Nagajyothi² · Dong Su Shin¹ · R. V. S. S. N. Ravikumar² · Jinsub Park^{1,3}

Received: 3 June 2015 / Accepted: 31 August 2015 / Published online: 7 September 2015
© Springer Science+Business Media New York 2015

Abstract Mn²⁺ doped ZnO nanopowder was prepared by simple sonochemical method. X-ray diffraction (XRD), scanning electron microscopy (SEM), energy dispersive X-ray (EDX) analysis, optical absorption (UV–Vis), photoluminescence (PL), Electron Paramagnetic Resonance (EPR), Fourier transform infrared (FT-IR) spectroscopy and magnetization have been used to characterize the sample. XRD study revealed that Mn²⁺ doped ZnO had wurtzite hexagonal structure. Composition analysis by EDX indicated the presence of small amounts of manganese. Crystal field (Dq) and interelectronic repulsion (B, C) parameters are evaluated from optical absorption. Spin-Hamiltonian and bonding parameters are evaluated from the EPR study. Optical and EPR confirms that the Mn²⁺ entered into ZnO lattice as distorted octahedral site symmetry. FT-IR spectrum exhibited vibrational bands of Zn–O bonds. PL spectrum shows the emission bands in UV and visible region. Magnetization loop was measured and clearly shows typical ferromagnetic saturation behavior. The results suggest oxygen vacancies, especially singly

ionized oxygen vacancies, play a crucial role in mediating ferromagnetism in the Mn doped ZnO system.

1 Introduction

Research on low-dimensional magnetic materials has been a focus because of their importance to biomedicine, non-linear optics and spin-based electronics in material science. The development of oxide based diluted magnetic semiconductors (DMS) with high Curie temperatures has attracted much attention in recent years because they show ferromagnetic state at room temperature (RTFM) [1]. Zinc oxide (ZnO), one of the very significant and adaptable semiconductor with direct band gap of ~3.37 eV and a large exciton binding energy of 60 meV at room temperature (RT) is a promising candidate for functional components of devices and materials in photonic crystals, gas sensors, light-emitting diodes, solar cells and photo electrochemical cells. ZnO materials are believed to be non-toxic, bio-safe and biocompatible [2] and have been used in many applications of daily life, such as drug carriers, cosmetics and fillings in medical materials [3]. It has high optical transparency in the visible range and it can be achieved through doping of transition metal (TM) ions in ZnO lattice [4]. Charge transfer between surface of nano-material and capping molecule can alter the electronic structure of nano-crystals and hence can boost the ferromagnetism in ZnO nanomaterials. Presence of defects due to large surface to volume ratio of nanomaterials allows tuning various properties which cannot be observed in their bulk form. Doping is the effective way to magically manipulate physical and optical properties of a wide band gap semiconductor. It is well known that doping a selective

Jinsub Park is a primary corresponding author and R. V. S. S. N. Ravikumar is a co-corresponding author.

✉ R. V. S. S. N. Ravikumar
rvssn@yahoo.co.in

✉ Jinsub Park
jinsubpark@hanyang.ac.kr

¹ Department of Electronics and Computer Engineering, Hanyang University, Seoul 133–791, Republic of Korea

² Department of Physics, University College of Sciences, Acharya Nagarjuna University, Nagarjuna Nagar, Guntur, Andhra Pradesh 522510, India

³ Department of Electronic Engineering, Hanyang University, Seoul 133–791, Republic of Korea

element into ZnO is the primary method for controlling the properties of semiconductor such as band gap or electrical conductivity, and to increase carrier concentration for electronic applications where a higher carrier concentration is required. The change of band gap is potential in transition metal ion doped ZnO leading to different colors of use for optical devices [5]. Transition metals have partially filled d states which can be used as doping elements for transforming spin frustrated semiconductors to ferromagnets. The quantum confinements on low-dimensional DMSs can be observed via optical characterization and their magnetic properties. Recently Babu et al. [6–10] have reported the synthesis and characterization various TM doped ZnO nanopowders with aid of ultrasonic waves. Among transition metals, Mn^{2+} doped ZnO system is an ideal DMS candidate and has been intensively investigated because Mn^{2+} atoms have largest magnetic moment. ZnO doped with Mn^{2+} has also been regarded as an ideal material for short wavelength magneto optical applications because of its wide band gap and the thermal solubility of Mn^{2+} in ZnO [11–13]. It can be concluded from previous reports that the magnetic properties of Mn^{2+} doped ZnO is very sensitive to native defects, surface states, chemical states and local environment of Mn^{2+} dopants.

2 Experimental details

Zinc acetate ($\text{Zn}(\text{CH}_3\text{COO})_2 \cdot 2\text{H}_2\text{O}$), Sodium Lauryl Sulphate (SLS) ($\text{C}_{12}\text{H}_{25}\text{O}_4\text{SNa}$), Manganese nitrate ($\text{Mn}(\text{NO}_3)_2$) and Sodium hydroxide (NaOH) are purchased from Merck Chemicals. All of the chemical reagents used in this experiment are analytical grade and used without further purification. The procedure employed for preparing ZnO nanopowder is as follows. In a typical synthesis, zinc acetate (2.195 g, 0.01 mol%) was grounded for 5 min and SLS (2.018 g, 0.007 mol%) was added to zinc acetate. After the mixture was grounded for another 5 min, it is stood for 2 h at RT. The mixture was still a solid powder then mixed with sodium hydroxide pellets (0.89 g, 0.02 mol%) and grounded again for 30 min. Later 0.03 mol% of manganese nitrate is added to the above mixture. The product is washed several times in an ultrasonic bath with distilled water and alcohol to remove any by-product and SLS. After washing, the solution is centrifuged at 10,000 rotations per minute about 30 min. The settled powder is collected and dried in air at 80 °C for 2 h.

Powder X-ray diffraction (XRD) pattern of Mn^{2+} doped ZnO powder was collected by PANalytical X'Pert Pro-diffractometer with $\text{CuK}\alpha$ radiation (1.5406 Å). Scanning Electron Microscope (SEM) and Energy Dispersive X-ray Spectroscopy (EDS/EDX) images were taken from JEOL JSM 6610 LV. Photoluminescence (PL) spectrum was

obtained from Horiba Jobin–Yvon Fluorolog-3 Spectrofluorimeter with Xe continuous (450 W) and pulsed (35 W) lamps as excitation sources. FT-IR spectrum was recorded using Shimadzu IRAffinity-1 FT-IR spectrometer in the region 400–4000 cm^{-1} . Optical absorption spectrum was taken from JASCO V-670 Spectrophotometer in the wavelength region of 200–1400 nm. The EPR spectrum was obtained from JEOL JES-TE100 ESR spectrometer operating at X-band frequencies and having a 100-kHz field modulation. The magnetic hysteresis loop was obtained from a Lake Shore 7407 vibrating sample magnetometer (VSM) for the sample.

3 Results and discussion

3.1 XRD study

The as synthesized product was subjected to XRD characterization for the identification of crystal structure. XRD confirmed that sample has hexagonal wurtzite structure of ZnO and corresponding pattern is shown in Fig. 1. No peaks belonging to Mn metal, Mn oxides or other impurity phases were detected. The peaks observed at $2\theta = 31.5577^\circ$, 34.2129° , 36.0394° , 47.3327° , 56.3881° , 62.6623° , 66.1534° , 67.7660° and 68.8610° are corresponds to the diffraction planes of ZnO (1 0 0), (0 0 2), (1 0 1), (1 0 2), (1 1 0), (1 0 3), (2 0 0), (1 1 2) and (2 0 1) respectively. Comparing the XRD data with standard wurtzite hexagonal structure of ZnO (JCPDS File No.36-1451), the peaks of diffraction pattern are shifted to lower diffraction angles, wider FWHM and increase of lattice cell parameters are well agreement with previous reports. From the XRD data, lattice cell parameters are evaluated as $a = 0.3260$, $c = 0.5226$ nm, when compared with standard values slightly increased ($a = 0.3249$, $c = 0.5206$ nm). This change in lattice parameters and shifts of peaks to lower angles can be attributed to Mn incorporation and is

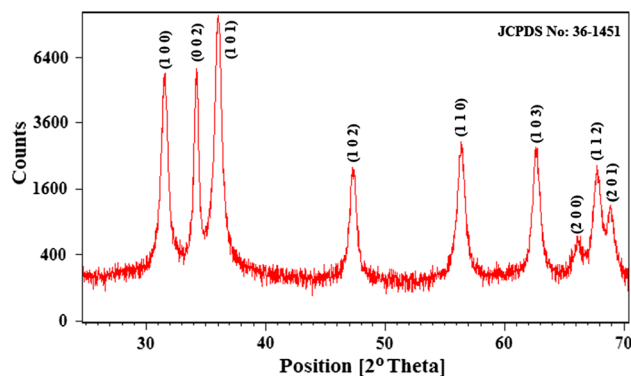


Fig. 1 X-ray diffraction of Mn^{2+} ions doped ZnO nanopowder

indicative of Mn doping into the ZnO matrix. The average crystallite size (t) of the Mn^{2+} doped ZnO nanopowder can be deduced from the XRD peaks using the Debye–Scherrer's formula [14]

$$t = 0.9\lambda/\beta \cos \theta$$

where λ is the X-ray wavelength, β is the full width at half maximum intensity (FWHM) and θ is the Bragg's angle. The average crystallite size was found to be around 21 nm.

3.2 Morphological study

SEM technique is used to study surface morphology and distribution of particles for the samples. In the present investigation, SEM images of Mn^{2+} doped ZnO nanopowder were shown in the Fig. 2a, b which are recorded at different magnifications. Micrographs revealed that the sample shows rough surface morphology. In addition, EDS results showed the weight percentage of dopant present in the host matrix in Fig. 3.

3.3 Optical absorption

Electronic configuration of Mn^{2+} (d^5) gives rise to free ion terms ${}^6\text{S}$, ${}^4\text{P}$, ${}^4\text{F}$, ${}^4\text{G}$, in addition to a number of doublet states of which ${}^6\text{S}$ occupies the ground state. ${}^6\text{S}$ and ${}^4\text{P}$ terms transform as ${}^6\text{A}_{1g}$ and ${}^4\text{T}_{1g}$ respectively, in crystal fields. ${}^4\text{D}$ and ${}^4\text{G}$ splits into ${}^4\text{E}_g + {}^4\text{T}_{2g}$ and ${}^4\text{A}_{1g} + {}^4\text{E}_g + {}^4\text{T}_{1g} + {}^4\text{T}_{2g}$ respectively [15]. The formation of Mn^{2+} doped ZnO nanopowder was confirmed by UV–Vis spectra. The optical absorption spectrum of prepared material from 200 to 600 nm is shown in Fig. 4. The spectrum shows various spin-forbidden d–d bands at 387, 420, 467 and 555 nm which are characteristics of octahedral site symmetry for Mn^{2+} . The bands are sharp, when the energy expressions for the transition are independent of Dq , whereas the bands are broad when they depend on Dq . The bands observed at around 387, 467 and 555 nm depend on crystal field parameter Dq and are assigned to the transitions ${}^6\text{A}_{1g}(\text{S}) \rightarrow {}^4\text{T}_{2g}(\text{D})$, ${}^6\text{A}_{1g}(\text{S}) \rightarrow {}^4\text{T}_{2g}(\text{G})$ and

${}^6\text{A}_{1g}(\text{S}) \rightarrow {}^4\text{T}_{1g}(\text{G})$ respectively; the band observed at around 420 nm is assigned to the transition ${}^6\text{A}_{1g}(\text{S}) \rightarrow {}^4\text{A}_{1g}(\text{G}) + {}^4\text{E}_g(\text{G})$, which is independent of Dq . These transitions are assigned using Tanabe–Sugano diagram [15]. The energy matrices for d^5 configuration with Tree's correction factor ($\alpha = 76 \text{ cm}^{-1}$) are solved for different sets of crystal field parameter Dq , Racah parameters B and C . The values which give good fit with observed data are $Dq = 750$, $B = 650$ and $C = 3150 \text{ cm}^{-1}$. The band head data along with calculated values are given in Table 1. The observed and calculated values of parameters are in good agreement with the reported system [16].

3.4 PL analysis

In general, the spectrum of ZnO exhibit three types of emissions i.e. ultraviolet, blue and green emissions. The ultraviolet emission of ZnO is generally attributed to exciton emission originating from recombination of free exciton through an exciton–exciton collision process [17]. The mechanism of blue emission is related to either oxygen vacancies or Zn vacancies [18] and green emission is commonly attributed to the transition of a photo-generated electron from a deep level below the conduction band to a deeply trapped hole resulting from an oxygen vacancy [19]. The crystal quality of synthesized nanopowder can affect origin and intensity of the UV emission and hence enhancement in the UV emission is observed for nanopowders with better crystal quality. Therefore the improvement of crystal quality (less structural defects and impurities, such as oxygen vacancies and Zn interstitials etc.) leads the sharp and strong origination of UV emission in the room temperature PL spectrum [20]. PL spectrum of as prepared Mn^{2+} doped ZnO nanopowder with an excitation wavelength of 325 nm shown in Fig. 5. The bands are observed in UV and visible region. The ultraviolet emission at 383 nm is due to exciton emission originating from recombination of free excitations through an exciton–

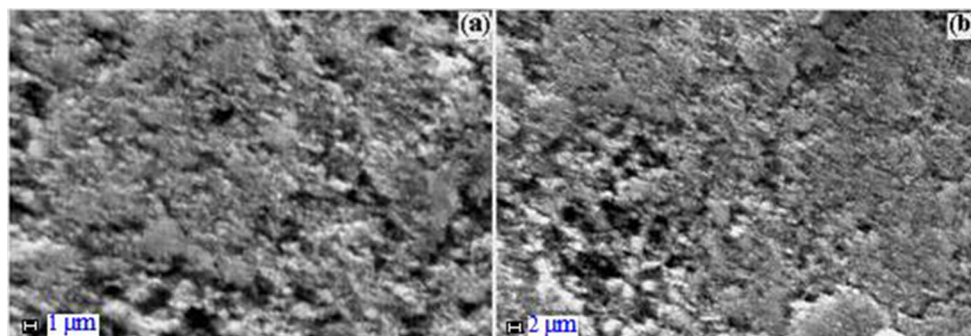


Fig. 2 SEM images of Mn^{2+} ions doped ZnO nanopowder

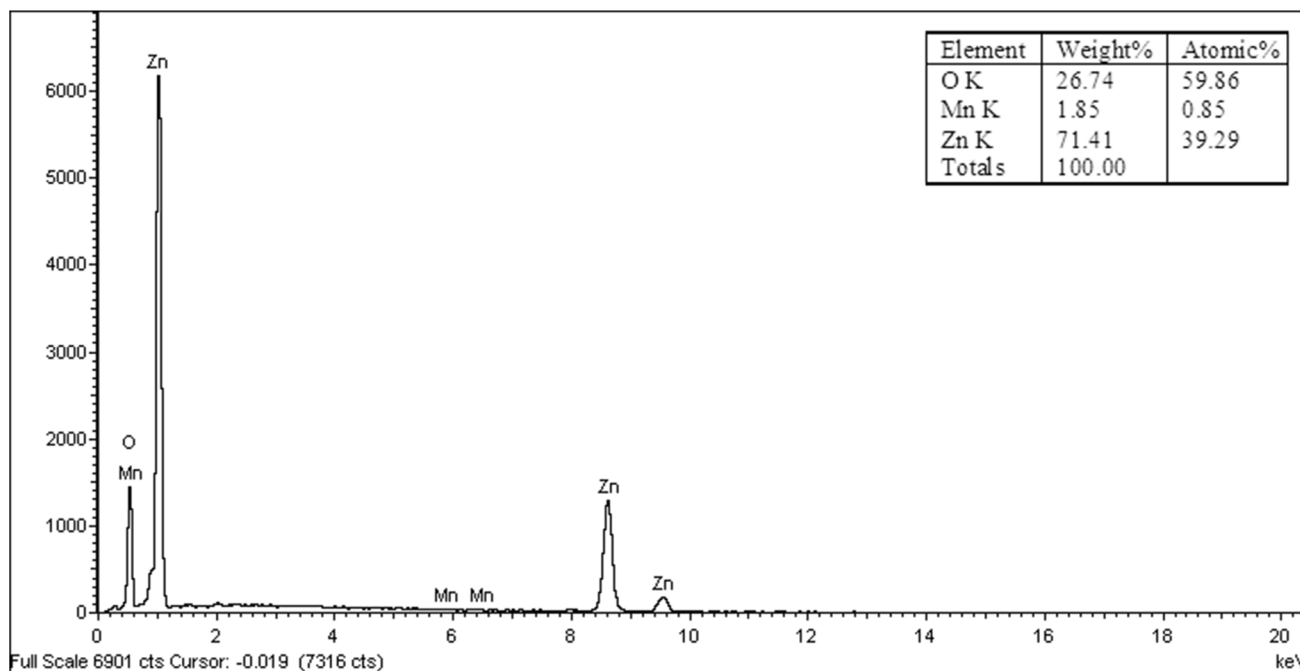


Fig. 3 EDS spectrum of Mn²⁺ doped ZnO nanopowder

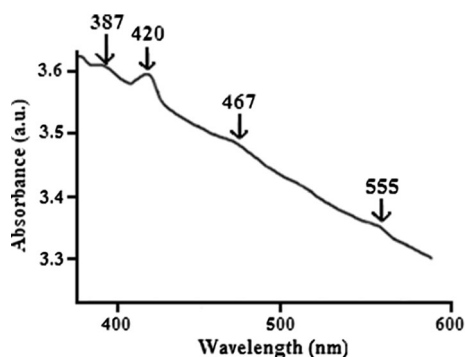


Fig. 4 Optical absorption spectrum of Mn²⁺ doped ZnO nanopowder

exciton collision process. The strong violet with corresponding weak blue emission bands around 425 and 467 nm are associated to oxygen or zinc vacancies. The transition of a photo generated electron of green emission band is observed at 505 nm. Finally strong band of yellow

to orange emission is occurred at 578 nm, characteristic emission of Mn²⁺ ascribed ⁴T₁–⁶A₁ transition in d shell, occupies the octahedral site symmetry in the host lattice [21]. CIE 1931 chromaticity coordinates were also calculated from the emission spectrum. In the present investigation the calculated values of chromaticity index can be written as (x = 0.3369, y = 0.3028). The corresponding diagram for chromaticity index is shown in Fig. 6. The circular spot on the Chromaticity diagram represents the corresponding emission colour in the white region. In order to inspect the quality of light, colour correlated temperature (CCT) values has been calculated from colour coordinates using McCamy empirical formula [22];

$$CCT = -437n^3 + 3601n^2 - 6861n + 5514.31$$

where $n = (x - x_e)/(y - y_e)$ and the chromaticity epicenter is at $x_e = 0.3320$ and $y_e = 0.1858$, (x, y) are calculated coordinates prepared samples. CCTs of Mn²⁺ ions

Table 1 Assignments of various transitions for optical absorption spectrum of Mn²⁺ doped ZnO nanopowder

Transitions from ⁶ A _{1g} (S)	Wavelength (nm)	Wavenumber (cm ⁻¹)		Dq (cm ⁻¹)	B (cm ⁻¹)	C (cm ⁻¹)
		Observed	Calculated			
⁴ T _{2g} (D)	387	25,839	25,857			
⁴ A _{1g} (G) + ⁴ E _g (G)	420	23,809	23,770	750	650	3150
⁴ T _{2g} (G)	467	21,413	21,432			
⁴ T _{1g} (G)	555	18,018	18,027			

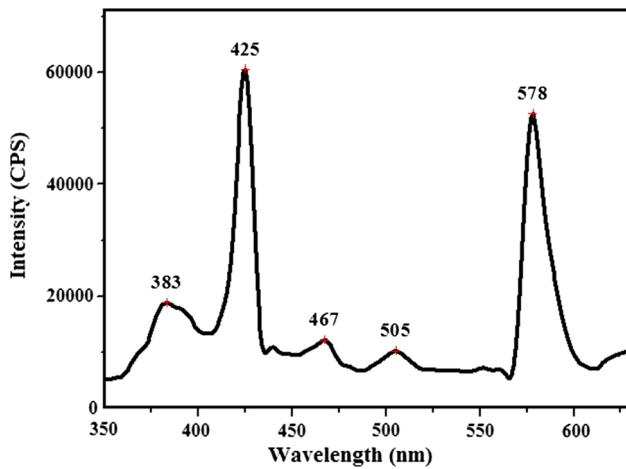


Fig. 5 PL spectrum of Mn²⁺ doped ZnO nanopowder

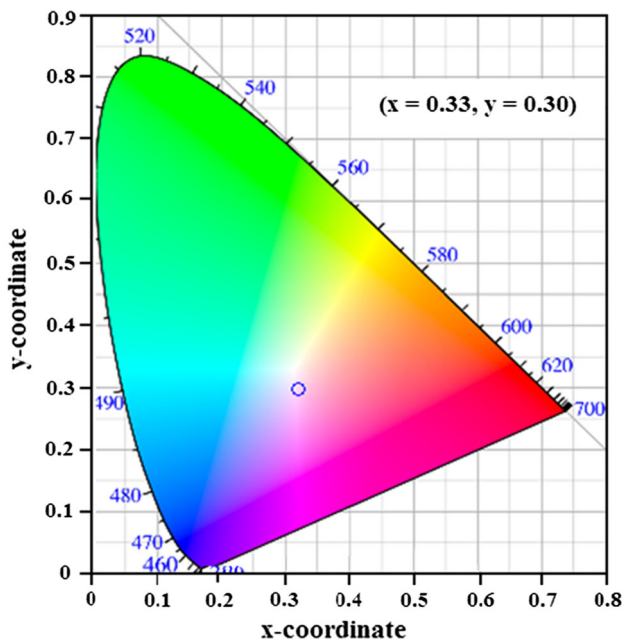


Fig. 6 CIE chromaticity diagram of Mn²⁺ doped ZnO nanopowder

doped ZnO nanopowder is 5231 K. Generally, CCT value >5000 K indicates the cold white light used for commercial lighting purpose and <5000 K indicates the warm white light used for home appliances [23]. Hence, this material may be used in white light display devices.

3.5 EPR study

EPR studies provide a detailed description of the ground state of the paramagnetic ions and enable to understand the nature of the site symmetry produced by the ligands around the transition metal ion. Mn²⁺ belongs to d⁵ configuration. It is well known in the case of Mn²⁺ that axial distortion of

octahedral symmetry gives rise to three Kramers' doublets, i.e., |±5/2>, |±3/2> and |±1/2>. Application of Zeeman field lifts the spin degeneracy of the Kramers' doublets [24]. As ⁵⁵Mn hyperfine interaction is large and very anisotropic in low-spin Mn²⁺ complexes, isotropic spectra tend to be poorly resolved and undiluted powders give very broad lines. EPR spectra of low-spin Mn²⁺ complexes have been elusive, in part because of high-spin Mn²⁺ decomposition products which have easily observed spectra. A typical X-band EPR spectrum, observed at room temperature for Mn²⁺ doped ZnO nanopowder, is shown in Fig. 7, which has broad lines centered at g = 2.0071, characteristic of octahedral site symmetry of Mn²⁺ within the framework material. The spin-Hamiltonian and bonding parameters are evaluated as g = 2.0071 and A = 90 cm⁻¹. In general, the g-value for the hyperfine splitting is indicative of the nature of the bonding. If the g-value shows a negative shift with respect to the free electron value (2.0023) then the bonding is ionic and conversely, if the shift is positive, then the bonding is more covalent. In the present case, the g-value shows positive, indicative of covalent bonding between Mn²⁺ and ligands [25]. Hence, the doped Mn²⁺ is ascribed to the octahedral site symmetry and partially covalent bonding with its ligands in ZnO host matrix.

3.6 FT-IR study

FT-IR spectrum of Mn²⁺ doped ZnO nanopowder shows the fundamental mode of vibrations at ~3400, ~2900, ~1400, and ~1600 cm⁻¹ which correspond to the O–H, C–H, asymmetric and symmetric C=O stretching modes respectively. The absorption bands in the range from 430 to 650 cm⁻¹ are attributed to the stretching modes of Zn–O [26, 27]. Hence the absorption bands at 609 cm⁻¹ is attributed to the stretching modes of ZnO. The FT-IR spectrum of Mn²⁺ doped ZnO nanopowder is shown in

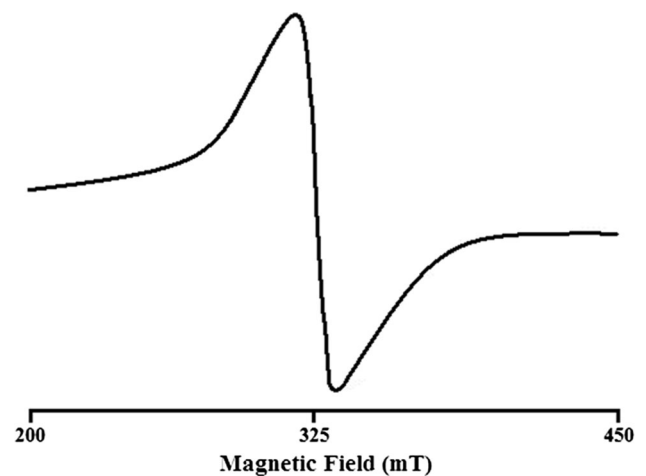


Fig. 7 EPR spectrum of Mn²⁺ doped ZnO nanopowder

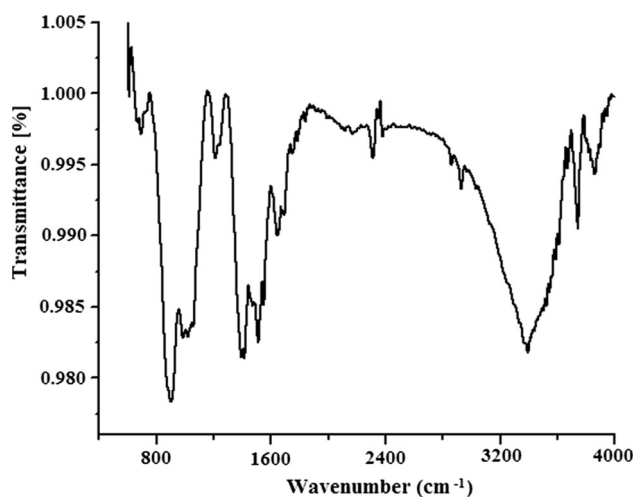


Fig. 8 FT-IR spectrum of Mn^{2+} doped ZnO nanopowder

Fig. 8. The absorption band at 3392 and 3745 cm^{-1} is due to the hydroxyl stretching O–H mode. The absorption peaks in the range of 2855 – 2930 cm^{-1} are attributed to the stretching band of C–H (alkyl group). The band observed at 2309 cm^{-1} is because of an existence of CO_2 molecule in air. The absorption peak at 1645 cm^{-1} is ascribed to H–O–H stretching band. The absorption band at 1506 cm^{-1} is attributed to the symmetric stretching mode of C=O and at about 1400 cm^{-1} can be assigned as asymmetric stretching mode of C=O. The overtone of ZnO is observed at 895 cm^{-1} which indicates the formation of tetrahedral coordination of Zn is present [28].

3.7 Magnetic study

Figure 9 shows magnetic hysteresis loop in M–H measurements performed for Mn^{2+} doped ZnO nanopowder at

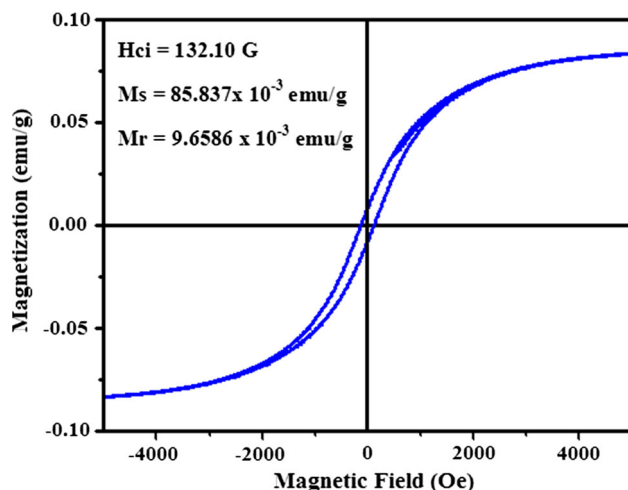


Fig. 9 Room temperature M–H curve of Mn^{2+} doped ZnO nanopowder

room temperature. The sample exhibits well defined hysteresis loop, which is indicative of room temperature ferromagnetic behavior. From the XRD analysis, the absence of secondary phase is confirmed. Saturation magnetization (M_s) of Mn^{2+} doped ZnO nanopowder is estimated to be about $85.83 \times 10^{-3}\text{ emu/g}$. The remnant magnetization (M_r) and coercive field (H_c) are $9.65 \times 10^{-3}\text{ emu/g}$ and 132.10 Oe , respectively. Two main factors probably lead to the appearance of ferromagnetism in TM doped ZnO nanocrystals: one is increase of the number of defects and oxygen vacancies. The second one is exchange interactions between TM ions and O ions spin moments. From above analysis, it can be conclude that the ferromagnetism in Mn^{2+} doped ZnO nanopowder is not from other impurities but expected to be intrinsic.

4 Conclusions

Mn^{2+} doped ZnO nanopowder is prepared successfully by simple sonochemical method. XRD measurements revealed the hexagonal wurtzite structured ZnO with Mn^{2+} with crystallite size of 21 nm without any other secondary phases. SEM images show rough surface morphology. The optical absorption spectrum shows the doped Mn^{2+} occupied at octahedral site symmetry for which crystal field (Dq) and interelectronic repulsion (B, C) parameters are evaluated. PL spectrum revealed that characteristic ZnO emission bands in UV region. The evaluated CIE colour coordinates indicated that this prepared sample may be used for white light emitting devices. From the EPR study, spin-Hamiltonian and bonding parameters are evaluated. By correlating optical and EPR data, Mn^{2+} entered into the ZnO lattice as distorted octahedral site symmetry. The nature of bonding between Mn^{2+} and its ligands is partially covalent. The FT-IR spectrum shows the formation of Zn–O bonds and showed the vibrational bands in the region of 600 – 4000 cm^{-1} . The magnetic hysteresis curve confirms the ferromagnetic nature at RT.

Acknowledgments This research was supported by the Basic Science Research Program of the National Research Foundation of Korea (NRF), funded by the Ministry of Education, Science and Technology (NRF-2015R1A1A1A05027848).

References

1. K. Sato, L. Bergqvist, J. Kudrnovský, P.H. Dederichs, O. Eriksson, I. Turek, B. Sanyal, G. Bouzerar, H. Katayama-Yoshida, V.A. Dinh, T. Fukushima, H. Kizaki, R. Zeller, *Rev. Mod. Phys.* **82**, 1633 (2010)
2. C. Cheng, G. Xu, H. Zhang, Y. Luo, *Mater. Lett.* **62**, 1617 (2008)

3. M.V. Limaye, S.B. Singh, R. Das, P. Poddar, S.K. Kulkarni, J. Solid State Chem **184**, 391 (2011)
4. W.Q. Peng, S.C. Qu, G.W. Cong, Z.G. Wang, Mater. Sci. Semicond. Process **9**, 156 (2006)
5. Y.S. Wang, J. Thomas, P. O'Brien, J. Phys. Chem. B **110**, 21412 (2006)
6. B. Babu, Ch. Rama Krishna, Ch. Venkata Reddy, V. Pushpa Manjari, R.V.S.S.N. Ravikumar, Spectrochim. Acta **109**, 90 (2013)
7. B. Babu, T. Aswani, G. Thirumala Rao, R. Joyce Stella, B. Jayaraja, R.V.S.S.N. Ravikumar, J. Magn. Magn. Mater **355**, 76 (2013)
8. B. Babu, V. Pushpa Manjari, T. Aswani, G. Thirumala Rao, R. Joyce Stella, R.V.S.S.N. Ravikumar, J. Phys **88**, 683 (2014)
9. B. Babu, G. Thirumala Rao, V. Pushpa Manjari, K. Ravindranadh, R. Joyce Stella, R.V.S.S.N. Ravikumar, J. Mater. Sci.: Mater. Electron **25**, 4179 (2014)
10. B. Babu, G. Rama Sundari, K. Ravindranadh, M. Rajesh Yadav, R.V.S.S.N. Ravikumar, J. Magn. Magn. Mater **372**, 79 (2014)
11. A. Ali Fatima, S. Devadason, T. Mahalingam, J. Mater. Sci.: Mater. Electron **25**, 3466 (2014)
12. C.H. Bates, W.B. White, R.J. Roy, Inorg. Nucl. Chem. Lett **28**, 397 (1966)
13. K. Omri, O. M. Lemine, J. El Ghoul, L. El Mir, J. Mater. Sci.: Mater. Electron. Doi [10.1007/s10854-015-3164-3](https://doi.org/10.1007/s10854-015-3164-3)
14. J. Elanchezhyan, J. Alloys Compd **468**, 7 (2009)
15. Y. Tanabe, S. Sugano, J. Phys. Soc. Jpn **9**, 753 (1954)
16. Ch. Rama, U. Udayachandran Thampy, D.V. Sathish, Ch. Venkata, A.V. Chandrasekhar, Y.P. Reddy, P.S. Rao, R.V.S.S.N. Ravikumar, J. Coord. Chem **64**, 4276 (2011)
17. D.J. Qiu, H.Z. Wu, A.M. Feng, Y.F. Yao, N.B. Chen, T.N. Xu, Appl. Surf. Sci **222**, 263 (2004)
18. S. Zhang, Y. Zhu, S. Zhu, Y. Chen, Thin Solid Films **515**, 2361 (2006)
19. Y. Dai, Y. Zhang, Y.Q. Bai, Z.L. Wang, Chem. Phys. Lett **375**, 96 (2003)
20. A. Umar, Y.B. Hahn, Nanotechnology **17**, 2174 (2006)
21. V. Pushpa Manjari, Ch. Rama, Sk Muntaz Begum, R.V.S.S.N. Ravikumar, Eur. Phys. J. Appl. Phys **65**, 10403 (2014)
22. C.S. McCamy, Color Res. Appl **17**, 142 (1992)
23. S.H. Lee, J.H. Park, S.M. Son, J.S. Kim, Appl. Phys. Lett **89**, 221916 (2006)
24. D.L. Griscom, J. Non-Cryst. Solids **40**, 211 (1980)
25. J.S. Van Wieringen, Discu. Faraday Soc **19**, 118 (1955)
26. R.D. Waldron, Phys. Rev **99**, 1727 (1955)
27. P.D. Cozzoli, M.L. Curri, A. Agostano, G. Leo, M. Lomascolo, J. Phys. Chem. B **107**, 4756 (2003)
28. S.P. Yawale, S.V. Pakade, Indian J. Pure Appl. Phys **33**, 34 (1995)